

SENSING EFFECTIVENESS OF PIEZOELECTRIC PATCHES WITH FINITE STIFFNESS BONDING

Alfredo R. de Faria

Instituto Tecnológico de Aeronáutica, Dept. Engenharia Mecânica, CTA-ITA-IEM, São José dos Campos, SP 12228-901
e-mail: arfaria@mec.ita.br

Abstract. *The impact of the quality of the bonding layer on the sensing capability of plane piezoelectric patches is assessed. The bonding layer between piezoelectric material and main structure is assumed to be elastic, having a finite stiffness and considerable thickness when compared to the thickness of the piezoelectric sensor. The equations governing the mechanical equilibrium are simplified by assuming a pure shear stress state in the bonding film. Starting with the strong form of the variational principle involved (equilibrium equations), the associated functional is obtained and, subsequently, the finite element method is employed to solve the governing equations in two dimensions. The displacements found are those occurring on the contact surface between bonding film and piezoelectric sensor. The numerical solution obtained in terms of displacements allows for the calculation of the effective voltage observed by the piezoelectric sensor. The results obtained by the finite element model developed are compared against those obtained by commercial codes for the particular case of zero voltage enforced.*

Keywords. *Piezoelectric material, sensors, bonding*

1. Introduction

Piezoelectric patches are now commonly used as actuators or sensors in many areas such as noise suppression, robotics, shape control and mechatronics (Tzou, 1991; Batra et al., 1996; Barrett, 1994). Accurate models for prediction of piezoelectric effects on structural responses have been and are still under development with increasingly complexity and refinement (Liao et al., 1991; Crawley et al., 1990).

Despite recent advancements, a number of non-idealities can be pointed out in real applications that are seldom taken into account in numerical models (de Faria et al., 1996; Crawley et al., 1987). The non-linearity of the constitutive equations is often disregarded although formulations that incorporate nonlinear strain-displacement relations are reasonably well documented (Meressi et al., 1993; Ha et al., Chang, 1992). Creep or strain rate effects may be significant and sometimes beneficial (active or passive damping applications (Trindade et al., 2000, Trindade et al., 2001) but are usually neglected. Other non-idealities may be listed such as depoling of piezoelectric material, electromechanical hysteresis, etc.

There are basically two types of strategies adopted when it comes to integrating the piezoelectric patches or layers to the main structure: bonding or embedding sensors/actuators. In both cases the interface between main structure and piezoelectric material play a decisive role in terms of strain/stress transfer mechanisms. A good interface ensures that effective actuation or sensing is achieved, avoiding the necessity of excessive voltages to be applied in the case of actuators and inaccurate output results in the case of sensors, thereby increasing robustness of control systems.

Investigations that consider the finite stiffness character of the interface or its thickness can be carried out without introducing the complications of some of the non-idealities cited earlier. Within the context of linear analyses it is possible to quantitatively assess the quality of the interface. The problem to be solved is essentially three-dimensional but it may be simplified to a two-dimensional one if no delamination or debonding is assumed. In this situation the assumption of a simplifying stress state in the interface can be adopted without serious loss of accuracy.

This work addresses the assessment of the quality of the bonding layer of piezoelectric sensors that are mounted on external surfaces of the main structure. Both external surface and piezoelectric patches are assumed to be perfectly plane and parallel, having a layer of adhesive joining them together. The assumption of a pure shear stress state occurring over the bonding layer is adopted such that the differential equilibrium equations can be simplified, i.e., the out-of-plane shear stresses are proportional to the in-plane displacements.

A full three-dimensional model is used to compare against the results obtained by the present two-dimensional model. In these comparisons the piezoelectric material is assumed to be under no voltage such that the electro-mechanical coupling is cancelled out. This allows for the use of traditional elements implemented in commercial finite element packages to be used despite the fact that, fundamentally, the problem involves both mechanical and electrical degrees of freedom.

2. Problem Formulation

The basic geometry involved in the formulation is illustrated in Fig. (1). The piezoelectric patch shown has a quadrilateral arbitrary shape but it is assumed to have a constant thickness h_p . The bonding layer (the shaded area) is also assumed to have a constant thickness h_b . It must be clear that both thicknesses are exaggerated in order to facilitate visualization. The dashed lines in Fig. (1) are parallel to the coordinate system xyz ; these are drawn to represent the surface on which the piezoelectric patch is mounted. The displacements u and v indicated in Fig. (1) are those measured

along the x and y axes, respectively, occurring on the surface between bonding and piezoelectric materials. The displacements \bar{u} and \bar{v} have orientations similar to u and v but occur on the surface between bonding layer and main structure.

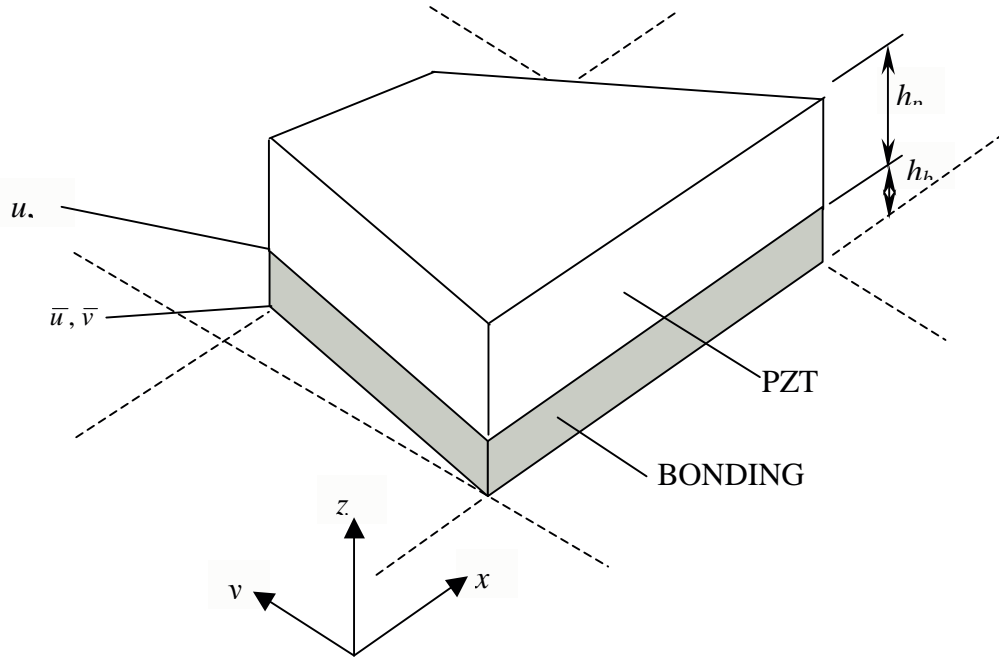


Figure 1. Basic geometry of piezoelectric patch

The assumption concerning the bonding layer is that it is in a state of pure shear such that stresses τ_{xz} and τ_{yz} are nonzero and independent of z . Admitting that the out-of-plane shear stresses vary linearly with z in the piezoelectric material the linear equations governing the equilibrium within the domain of the piezoelectric material may be expressed as

$$\frac{\partial \sigma_{xx}}{\partial x} + \frac{\partial \tau_{xy}}{\partial y} - \frac{\tau_{xz}}{h_p} = 0 \quad (1a)$$

$$\frac{\partial \sigma_{yy}}{\partial y} + \frac{\partial \tau_{xy}}{\partial x} - \frac{\tau_{yz}}{h_p} = 0 \quad (1b)$$

$$\frac{\partial D_z}{\partial z} = 0 \quad (1c)$$

where D_z is the electrical displacement in the z direction. Eqs. (1a-b) are mechanical equilibrium equations in the x and y directions respectively. Equation (1c) is the electrical equilibrium derived from Maxwell's equations. Notice that the constitutive equations have not been introduced yet but the electro-mechanical coupling leads to the occurrence of electrical variables in Eqs. (1a-b) and mechanical variables in Eq. (1c).

The shear stresses τ_{xz} and τ_{yz} can be computed from the assumption of a state of pure shear in the bonding layer as below:

$$\tau_{xz} = G_b \frac{(u - \bar{u})}{h_b}, \quad \tau_{yz} = G_b \frac{(v - \bar{v})}{h_b} \quad (2)$$

where G_b is the shear modulus of the bonding material. The variational principle associated with the equilibrium equations can now be stated as in Eq. (3).

$$\begin{aligned} \delta \Pi = & \int_{\Omega} h_p [\sigma_{xx,x} + \tau_{xy,y} - \frac{G_b}{h_b h_p} (u - \bar{u})] \delta u d\Omega + \\ & \int_{\Omega} h_p [\sigma_{yy,y} + \tau_{xy,x} - \frac{G_b}{h_b h_p} (v - \bar{v})] \delta v d\Omega + \int_{\Omega} \int_0^{h_p} D_{z,z} \delta \phi dz d\Omega \end{aligned} \quad (3)$$

where the shorthand notation $\partial/\partial x=(\cdot)_{,x}$ has been used, ϕ is the electric potential and Ω is the surface in between bonding layer and piezoelectric patch. Using Green's theorem in Eq. (3) yields

$$\begin{aligned} \delta\Pi = & -\int_{\Omega} h_p [\sigma_{xx} \delta u_{,x} + \tau_{xy} \delta u_{,y} + \frac{G_b}{h_b h_p} (u - \bar{u}) \delta u] d\Omega - \\ & -\int_{\Omega} h_p [\sigma_{yy} \delta v_{,y} + \tau_{xy} \delta v_{,x} + \frac{G_b}{h_b h_p} (v - \bar{v}) \delta v] d\Omega + \int_{\Omega} h_p D_z \delta E_z d\Omega + \\ & + \int_{\Omega} h_p (\sigma_{xx} n_x + \tau_{xy} n_y) \delta u d\Gamma + \int_{\Omega} h_p (\tau_{xy} n_x + \sigma_{yy} n_y) \delta v d\Gamma + \int_{\Omega} [D_z \delta \phi]_0^{h_p} d\Omega \end{aligned} \quad (4)$$

where $\bar{\Omega}$ is the boundary of Ω , $\mathbf{n} = (n_x, n_y)$ is the unit normal vector on $\bar{\Omega}$ and $E_z = -\phi_{,z}$ is the electric field along z .

It is now necessary to call upon the constitutive equations of the piezoelectric material. In this particular situation the constitutive equations can be used in two dimensions such that it is written as in Eq. (5)

$$\begin{Bmatrix} \sigma_{xx} \\ \sigma_{yy} \\ \tau_{xy} \\ D_z \end{Bmatrix} = \frac{E_p}{1-\nu_p^2} \begin{bmatrix} 1 & \nu_p & 0 & -e_{31} \\ \nu_p & 1 & 0 & -e_{32} \\ 0 & 0 & \frac{1-\nu_p}{2} & 0 \\ e_{31} & e_{32} & 0 & \zeta_{zz} \end{bmatrix} \begin{Bmatrix} \epsilon_{xx} \\ \epsilon_{yy} \\ \gamma_{xy} \\ E_z \end{Bmatrix} \quad (5)$$

where E_p and ν_p are, respectively, the modulus of elasticity and Poisson ratio of the piezoelectric material, e_{31} and e_{32} are piezoelectric constants that can be obtained from the coupling matrix $[d]$ (Allik, Hughes, 1970) and ζ_{zz} is the reduced dielectric constant. ϵ_{xx} , ϵ_{yy} , γ_{xy} are the usual linear mechanical deformations and E_z is the electric field along the z direction.

Substitution of Eq. (5) into (4) and dropping the boundary condition terms leads to the variational principle given in Eq. (6).

$$\begin{aligned} \delta\Pi = & -\int_{\Omega} h_p [(u_{,x} + \nu_p v_{,y}) \delta u_{,x} + (v_{,y} + \nu_p u_{,x}) \delta v_{,y}] \frac{E_p}{1-\nu_p^2} d\Omega - \\ & \int_{\Omega} h_p (u_{,x} + \nu_p v_{,y}) (\delta u_{,y} + \delta v_{,x}) G_p d\Omega + \int_{\Omega} (e_{31} \delta u_{,x} + e_{32} \delta v_{,y}) V d\Omega - \\ & \int_{\Omega} \frac{G_b}{h_b} (u \delta u + v \delta v) d\Omega + \int_{\Omega} \frac{G_b}{h_b} (\bar{u} \delta u + \bar{v} \delta v) d\Omega + \\ & \int_{\Omega} (e_{31} u_{,x} + e_{32} v_{,y}) \delta V d\Omega + \int_{\Omega} \frac{\zeta_{zz}}{h_p} V \delta V d\Omega \end{aligned} \quad (6)$$

where $E_z = V/h_p$. The scaled functional Π^* is obtained dividing Eq. (6) by $-E_p h_p / (1-\nu_p^2)$.

$$\begin{aligned} \Pi^* = & \frac{1}{2} \int_{\Omega} (u_{,x}^2 + v_{,y}^2 + 2\nu_p u_{,x} v_{,y}) d\Omega + \frac{1}{2} \int_{\Omega} \frac{(1-\nu_p)}{2} (u_{,y}^2 + v_{,x}^2 + 2u_{,y} v_{,x}) d\Omega + \\ & \frac{1}{2} \int_{\Omega} \frac{\Gamma^2}{A_{\Omega}} (u^2 + v^2) d\Omega - \int_{\Omega} \frac{\Gamma^2}{A_{\Omega}} (\bar{u} u + \bar{v} v) d\Omega - \\ & \int_{\Omega} (e_{31} u_{,x} + e_{32} v_{,y}) \frac{V(1-\nu_p^2)}{E_p h_p} d\Omega - \frac{1}{2} \int_{\Omega} \frac{\zeta_{zz} (1-\nu_p^2)}{E_p h_p^2} V^2 d\Omega \end{aligned} \quad (7)$$

where A_{Ω} is the area of the domain Ω and Γ is defined in Eq. (8).

$$\Gamma^2 = \frac{G_b(1-\nu_p^2)A_\Omega}{E_p h_b h_p} \quad (8)$$

It is clear from Eq. (8) that Γ is non-dimensional. Moreover, from the derivation of Eq. (7), it is understood that Γ reflects the contribution of the bonding layer finite stiffness to the problem functional Π^* . The higher Γ , the more the solution of the minimization of Π^* tends to $u = \bar{u}$, $v = \bar{v}$. Parameter Γ provides, therefore, a measure of the quality of the bonding layer.

3. The Finite Element Method

The functional presented in Eq. (7) must be minimized in order to obtain the solutions u and v . This is done numerically through the finite element technique. First derivatives of both u and v with respect to x and y are present suggesting that C^0 elements are used. Hence, the domain Ω is discretized into bilinear elements of four nodes with the aid of the interpolation functions defined in Eq. (9).

$$\begin{aligned} u &= \frac{1}{4} \begin{bmatrix} (1-\xi)(1-\eta) & (1+\xi)(1-\eta) & (1-\xi)(1+\eta) & (1+\xi)(1+\eta) \end{bmatrix} \{q_u\} = \mathbf{N}\mathbf{u}_e \\ v &= \frac{1}{4} \begin{bmatrix} (1-\xi)(1-\eta) & (1+\xi)(1-\eta) & (1-\xi)(1+\eta) & (1+\xi)(1+\eta) \end{bmatrix} \{q_v\} = \mathbf{N}\mathbf{v}_e \end{aligned} \quad (9)$$

where \mathbf{u}_e and \mathbf{v}_e are the nodal displacements u and v of element e . By inspection of Eq. (7) it is readily observed that the displacements \bar{u} , \bar{v} must be available. This is the case when the piezoelectric patch is used for sensing purposes because \bar{u} , \bar{v} are nothing but the displacements in the x and y direction at the surface of the main structure. Assuming a constant voltage V over the piezoelectric patch leads to the discretized functional Π_{FEM}^* expressed in Eq. (10) where n is the total number of bilinear elements.

$$\begin{aligned} \Pi_{\text{FEM}}^* &= \frac{1}{2} \sum_{e=1}^n \begin{Bmatrix} \mathbf{u}_e \\ \mathbf{v}_e \end{Bmatrix}^T \left(\int_{\Omega_e} \begin{bmatrix} \mathbf{N}_{,x}^T \mathbf{N}_{,x} & \nu_p \mathbf{N}_{,x}^T \mathbf{N}_{,y} \\ \nu_p \mathbf{N}_{,y}^T \mathbf{N}_{,x} & \mathbf{N}_{,y}^T \mathbf{N}_{,y} \end{bmatrix} d\Omega \right) \begin{Bmatrix} \mathbf{u}_e \\ \mathbf{v}_e \end{Bmatrix} + \\ &\frac{1}{2} \left(\frac{1-\nu_p}{2} \right) \sum_{e=1}^n \begin{Bmatrix} \mathbf{u}_e \\ \mathbf{v}_e \end{Bmatrix}^T \left(\int_{\Omega_e} \begin{bmatrix} \mathbf{N}_{,y}^T \mathbf{N}_{,y} & \mathbf{N}_{,y}^T \mathbf{N}_{,x} \\ \mathbf{N}_{,x}^T \mathbf{N}_{,y} & \mathbf{N}_{,x}^T \mathbf{N}_{,x} \end{bmatrix} d\Omega \right) \begin{Bmatrix} \mathbf{u}_e \\ \mathbf{v}_e \end{Bmatrix} + \\ &\frac{\Gamma^2}{2} \sum_{e=1}^n \begin{Bmatrix} \mathbf{u}_e \\ \mathbf{v}_e \end{Bmatrix}^T \left(\int_{\Omega_e} \frac{1}{A_\Omega} \begin{bmatrix} \mathbf{N}^T \mathbf{N} & \mathbf{0} \\ \mathbf{0} & \mathbf{N}^T \mathbf{N} \end{bmatrix} d\Omega \right) \begin{Bmatrix} \mathbf{u}_e \\ \mathbf{v}_e \end{Bmatrix} - \Gamma^2 \sum_{e=1}^n \begin{Bmatrix} \mathbf{u}_e \\ \mathbf{v}_e \end{Bmatrix}^T \left(\int_{\Omega_e} \frac{1}{A_\Omega} \begin{Bmatrix} \mathbf{N}^T \bar{u} \\ \mathbf{N}^T \bar{v} \end{Bmatrix} d\Omega \right) - \\ &\left(\frac{1-\nu_p^2}{E_p h_p} \right) \sum_{e=1}^n \begin{Bmatrix} \mathbf{u}_e \\ \mathbf{v}_e \end{Bmatrix}^T \left(\int_{\Omega_e} \begin{Bmatrix} e_{31} \mathbf{N}_{,x}^T \\ e_{32} \mathbf{N}_{,y}^T \end{Bmatrix} d\Omega \right) V - \frac{1}{2} \frac{A_\Omega \zeta_{zz} (1-\nu_p^2)}{E_p h_p^2} V^2 \end{aligned} \quad (10)$$

Assembly of the element matrices into global arrays allows one to write the system of equations that will give the solutions u and v . In a compact form these may be expressed as

$$\begin{bmatrix} \mathbf{K}_{qq} + \Gamma^2 \mathbf{K}'_{qq} & \mathbf{K}_{qV} \\ \mathbf{K}_{qV}^T & K_{VV} \end{bmatrix} \begin{Bmatrix} \mathbf{q} \\ V \end{Bmatrix} = \begin{Bmatrix} \Gamma^2 \bar{\mathbf{F}} \\ 0 \end{Bmatrix} \quad (11)$$

where \mathbf{q} is the global vector of displacements. Matrix \mathbf{K}_{qq} , relates to the first and second integrals in Eq. (10), matrix \mathbf{K}'_{qq} relates to the third integral in Eq. (10), vector $\bar{\mathbf{F}}$ relates to the fourth integral in Eq. (10) and matrix \mathbf{K}_{qV} relates to the fifth integral in Eq. (10). Notice that both K_{VV} and V are scalar quantities, and \mathbf{K}_{qV} is a column matrix. Once \mathbf{q} is determined from the solution of Eq. (11) the voltage read by the piezoelectric sensor is easily found making $V = -\mathbf{q}^T \mathbf{K}_{qV} / K_{VV}$.

4. Model Validation

The two-dimensional finite element model developed in the preceding section is compared against a three-dimensional finite element model implemented in the commercial code Nastran. Since electrical degrees of freedom are not formulated in Nastran one must be able to avoid its effects on the response of piezoelectric materials in order to provide a fair comparison with the finite element model implemented in this work. This is done by enforcing $V=0$ V in Eq. (11). In this manner the contribution of the electro-mechanical coupling matrix \mathbf{K}_{qV} is artificially cancelled out.

An important point that arises in modelling such thin films is that of element aspect ratio. In practical applications the thicknesses of both bonding and piezoelectric layers are very small when compared to the other dimensions of the layered structure in the xy plane. Thus, a large number of elements must be used along those directions when compared to the number of elements in the z direction. Moreover, due to the St. Venant principle, large strain gradients are expected to occur in the regions near the patch edges as opposed to small gradients in the central portion. Hence, mesh refinement is desired near the edges.

The material properties used in this work are given in Tab. (1). The validation of the code assumes that the bonding layer thickness is $h_b=200$ μm and that the piezoelectric layer has thickness $h_p= 200$ μm . This bonding layer thickness is too large for practical values but is used only for validation. A rectangular piezoelectric patch will be considered that has 5 cm side in the x direction and 2.5 cm side in the y direction. For this configuration $\Gamma=24.0$.

Table 1. Material properties

property	piezoelectric	bonding
Modulus of elasticity (GPa)	63.0	3.834
Poisson ratio	0.30	0.50
Shear modulus (GPa)	24.23	1.278
Piezoelectric constant e_{31} (N/Vm)	22.86	-
Piezoelectric constant e_{32} (N/Vm)	22.86	-
Reduced dielectric, ζ_{zz} (nC/Vm)	3.39	-

Three meshes were used in the calculations. Figure (2) shows a top view of the mesh used in the simulations for the present finite element model discussed in the previous section; it is refined near the edges and has 120 2D elements in the x direction unevenly spaced and 60 2D elements in the y direction also unevenly spaced. Two Nastran meshes were used, both having 120 solid elements in the x direction evenly spaced and 60 solid elements in the y direction evenly spaced. However, one out of those two meshes uses 1 solid element to represent bonding and 1 to represent piezoelectric layer in the z direction while the other uses 2 solid element to represent bonding and 2 to represent piezoelectric layer in the z direction. Thus, the Nastran meshes have 14,400 or 28,800 solid elements.

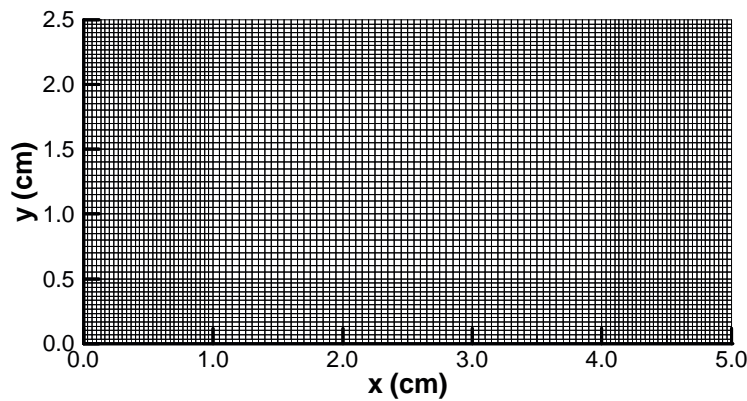


Figure 2. Finite element mesh used in the present model

Two simulations are conducted that reflect the strain distributions on the external surface of the main structure: (i) uniform normal strain in the x and y directions of $\epsilon_{xx}=50$ $\mu\epsilon$ and $\epsilon_{yy}=40$ $\mu\epsilon$ and (ii) pure shear in the xy plane of 30 $\mu\gamma$. In the present finite element model as well as in Nastran's prescribed displacements \bar{u} , \bar{v} are enforced that represent these strain states.

Figures (3a-d) show the strain distributions obtained along the patch center lines. Normal strains are shown in Figs. (3a) and (3b) and shear strains are shown in Figs. (3c) and (3d). It can be noticed that results for the finer Nastran mesh and the 2D mesh used in the present formulation (Fig. (2)) produce the same results whereas the coarser Nastran mesh displays distortions due to poor refinement along z .

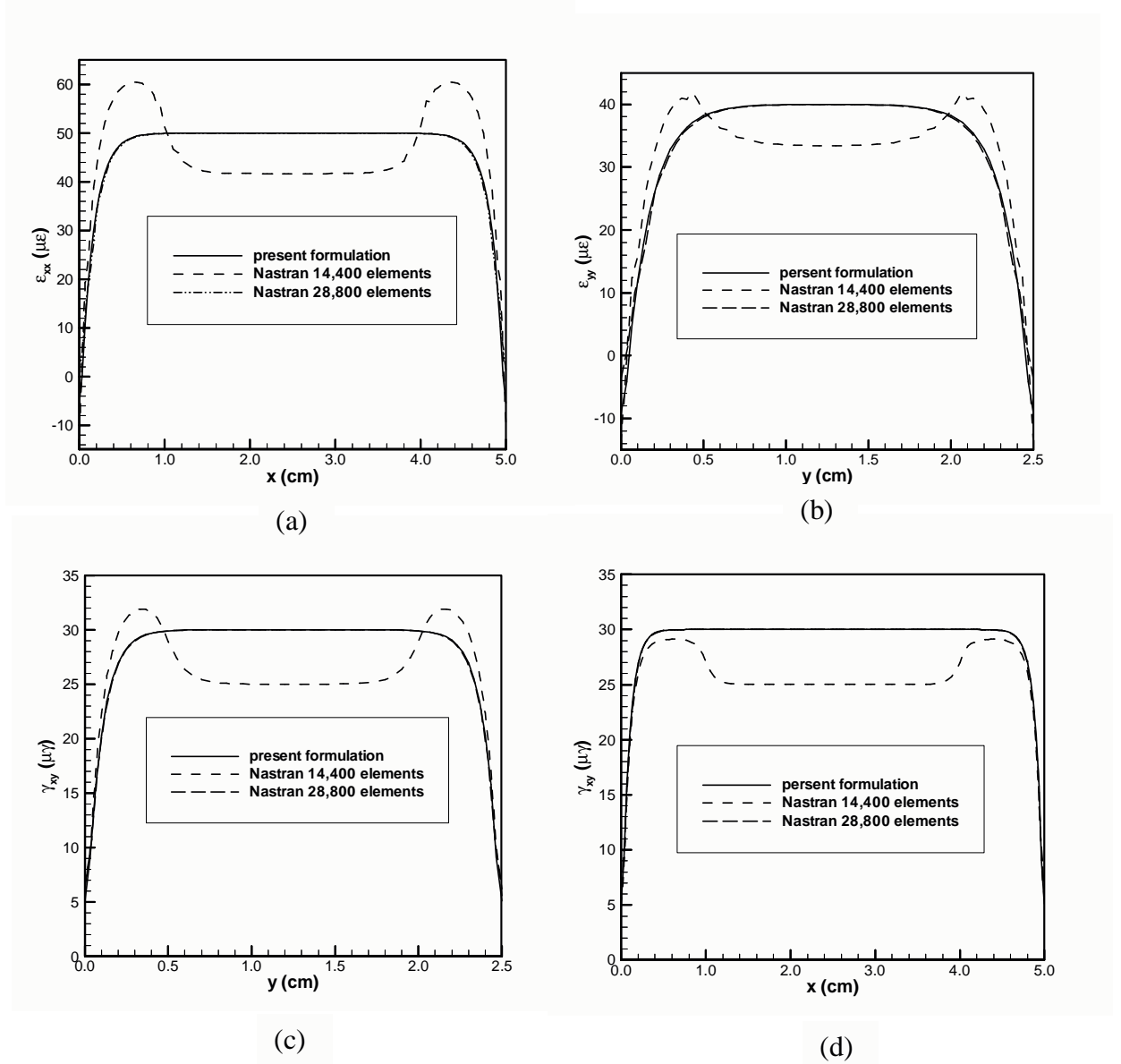


Figure 3. Strain distribution for validation

The more interesting comparison is that of total number of degrees of freedom. Accounting for just translation displacements in the finer Nastran mesh a total of 110,715 degrees of freedom are involved. In the present model 14,762 degrees of freedom are necessary, i.e., only 13.4% of Nastran's. The enforcement of $V=0$ V allowed one to use Nastran elements in this particular validation model. However, if V is free to vary the full matrix Eq. (10) must be solved what required knowledge of coupling matrix \mathbf{K}_{qV} and the electric matrix K_{VV} .

$$\begin{aligned}
 (\mathbf{K}_{qq} + \Gamma^2 \mathbf{K}'_{qq} - \mathbf{K}_{qV} K_{VV}^{-1} \mathbf{K}_{qV}^T) \mathbf{q} &= \Gamma^2 \bar{\mathbf{F}} \\
 V &= -K_{VV}^{-1} \mathbf{K}_{qV}^T \mathbf{q}
 \end{aligned} \tag{12}$$

5. Numerical Simulations and Discussion

The objective of the numerical simulations conducted is to assess the impact of the quality of the bonding layer on the effectiveness of piezoelectric sensors. It was shown that parameter Γ defined in Eq. (8) provides an adequate means of measuring the quality of the bonding film. Moreover, it is important to compare the actual voltage read by the piezoelectric sensors against the ideal voltage that would be observed when Γ increases without bounds ($\Gamma \rightarrow \infty$).

In the first simulation the same configuration and mesh used in the validation is adopted except that the thickness of the bonding layer is varied in order to represent different bonding stiffness. h_b is considered to be in between 1 μm

($\Gamma=339.7$) and $500 \mu\text{m}$ ($\Gamma=15.2$). Normal strains of $\varepsilon_{xx}=50 \mu\text{e}$ and $\varepsilon_{yy}=40 \mu\text{e}$ are imposed. If a perfect bond is assumed than the voltage observed under this strain state is $V_{\infty}=121.5 \text{ V}$.

The normalized voltage with respect to V_{∞} is shown in Fig. (4) for different values of Γ . For $\Gamma>120$ the effectiveness is more than 98%. This range of Γ corresponds to bonding film thicknesses not larger than $8 \mu\text{m}$ only which is very small for practical applications. A more realistic thickness of $100 \mu\text{m}$ gives $\Gamma=33.9$ and an effectiveness of 92%.

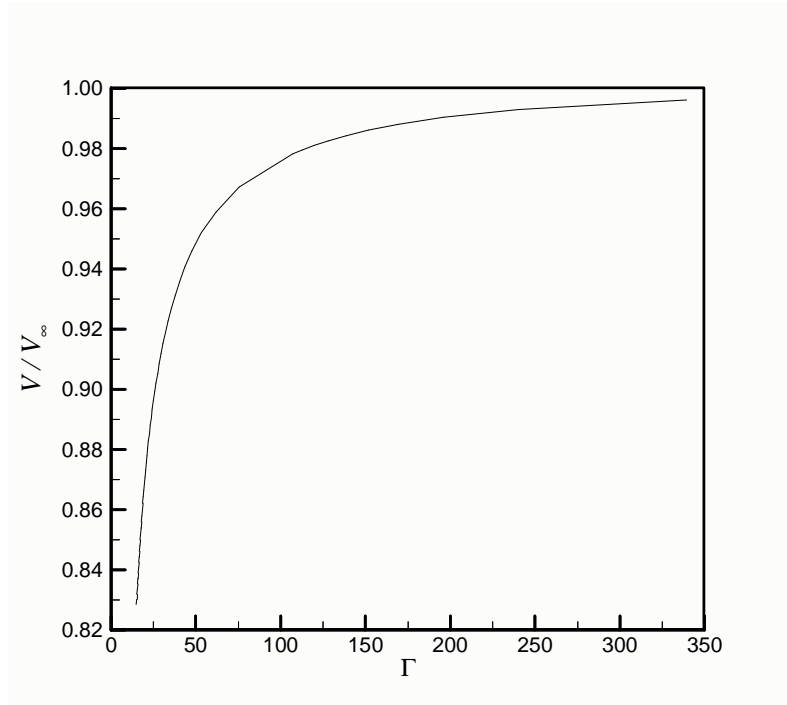


Figure 4. Effectiveness variation for rectangular piezoelectric sensors

The constitutive law given by equation (5) does not assume that the shear strain γ_{xy} contributes to the electric displacement D_z . The practical effect of this is that shear strains do not produce voltage in the piezoelectric sensor. Therefore, shear strains cannot be directly measured with a sensor patch made of that kind of piezoelectric material. The solution to circumvent this difficulty is to use more than one sensor to configure a network of sensors.

In a second simulation the shape of the piezoelectric patch is modified and its impact on the sensor effectiveness is assessed. The basic shape considered is that of a parallelogram whose sides are 5 cm and 2.5 cm long with an arbitrary angle α of inclination between them. Thicknesses are fixed at $h_p=200 \mu\text{m}$ and $h_b=100 \mu\text{m}$. The displacement field imposed \bar{u} , \bar{v} is representative of uniform normal strains $\varepsilon_{xx}=50 \mu\text{e}$ and $\varepsilon_{yy}=40 \mu\text{e}$. The mesh used is similar to that of Fig. (2) but the element sides are aligned with the parallelogram sides. The expression for Γ given in Eq. (8) this case can be slightly modified to accommodate the variable shape

$$\Gamma^2 = \frac{G_b(1-\nu_p^2)\bar{A}_\Omega}{E_p h_b h_p} \sin \alpha \quad (12)$$

where \bar{A}_Ω is the area of the rectangular shape (in this case 12.5 cm^2).

Figure (5) presents the plotting of the voltage observed V and the voltage V_{∞} that would be observed in a perfect bonding situation. The higher the distortion of the piezoelectric patch given by α , the smaller Γ . Hence, it is noticed that the strains imposed lead to the highest V for distorted shapes. However, the ideal voltage V_{∞} is also the highest for small α .

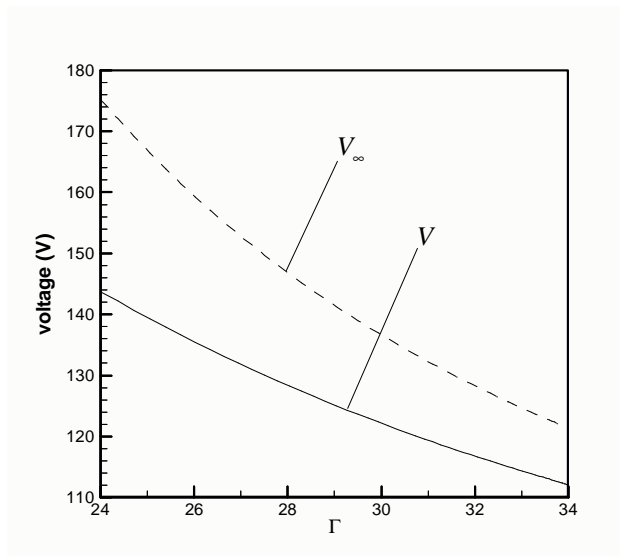


Figure 5. Output voltage for parallelogram shaped piezoelectric sensors

In order to assess the effectiveness it is important to compare the ratio V/V_∞ as was done in Fig. (4) To this end Fig. (6) is drawn where effectiveness is plotted against Γ . Observe now that V/V_∞ increases with Γ , i.e., a better sensor efficiency is obtained for larger Γ as expected. Simultaneous comparison of Figs. (5) and (6) shows that the best efficiency is obtained with high Γ but the disadvantage is that with higher Γ comes lower voltages.

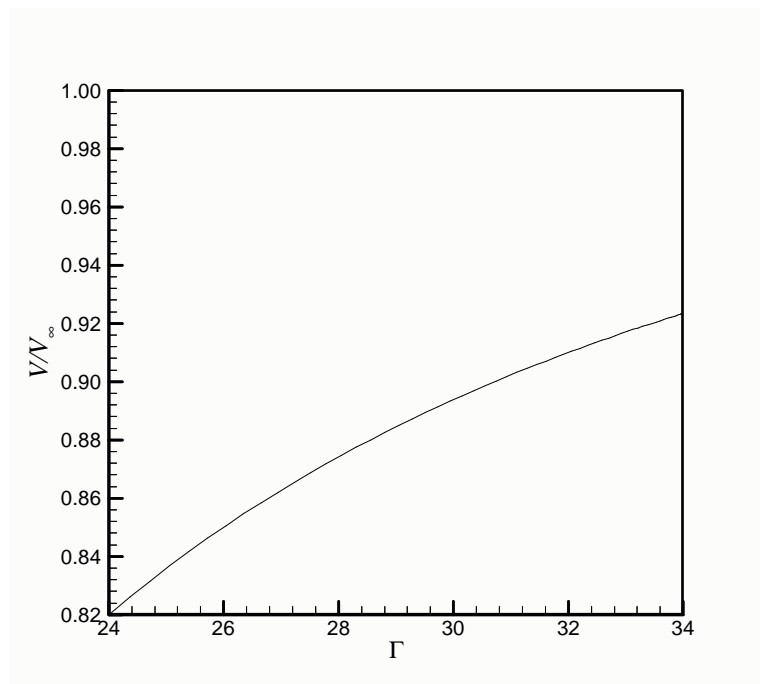


Figure 6. Effectiveness variation for parallelogram shaped piezoelectric sensors

Figure (5) reveals a very interesting result: distorted shapes produce higher voltages. This may not be a feature sought in piezoelectric sensors but it is certainly a relevant point when piezoelectric actuators are designed. In order to induce the same kind of strain distribution on the main structure one must impose higher voltages in distorted shapes of patches. This assertion is obviously valid only with regard to the parallelogram shaped patches. It may be possible, through shape optimization, to find a better distribution of piezoelectric material such that the smallest V is achieved given weight constraints for the same induced strains.

The mechanism behind loss of efficiency of piezoelectric sensors can be better understood if the strain distribution of a typical configuration is observed. The geometry used in the validation is assumed again but the bonding film thickness is $h_b=100 \mu\text{m}$ and normal strains of $\epsilon_{xx}=50 \mu\epsilon$ and $\epsilon_{yy}=40 \mu\epsilon$ are imposed in a rectangular patch. The strain distributions ϵ_{xx} , ϵ_{yy} and γ_{xy} are shown, respectively, in Figs. (7a), (7b) and (7c). The interesting remark is that in the central portion of the patch the strains are the same as those imposed. However, large gradients appear near the edges and the strains drop sharply. The edge effects are therefore the main reason for loss of efficiency.

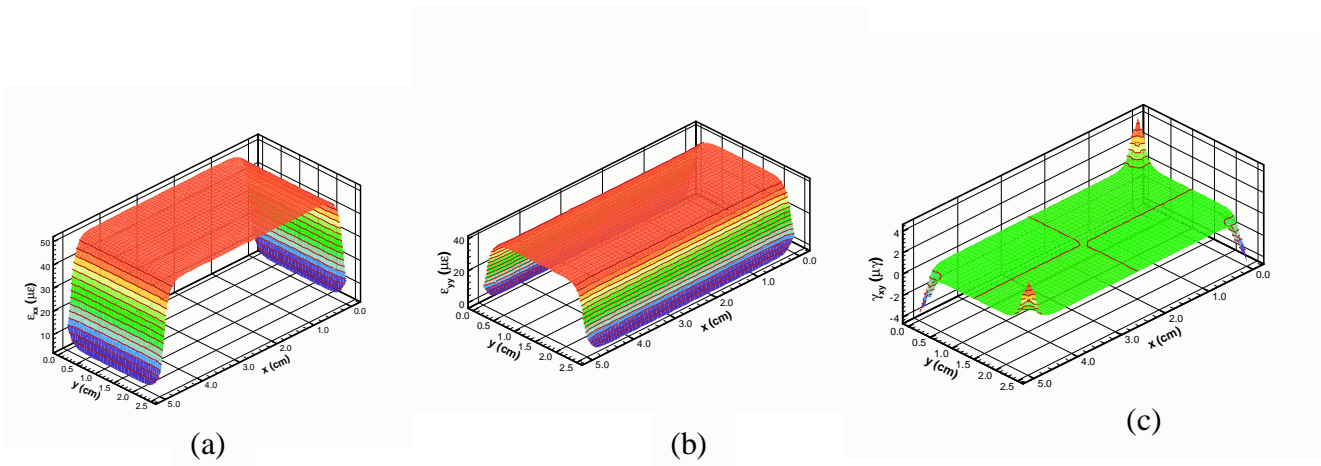


Figure 7. Typical strain distributions

The pure shear state assumed to exist within the bonding layer was shown to be an accurate approximation of the real strain distribution as proven by a 3D finite element model. Such assumption is useful in the analysis of piezoelectric patches because of the small thicknesses involved. However, as layers become thicker, the approximation deteriorates and alternative approaches should be used.

Debonding is not a concern in the present model. However, transverse strains may develop in the z direction that lead to that kind of failure. In order to capture that behavior a more refined finite element model can be used where a quasi-3D approach is employed (Nabarrete, 2002). In this case the displacements are also interpolated in the z direction and at least two layers of nodes must be used to represent that variation. The resulting model is able to predict transverse strains and stresses.

6. Conclusions

The present investigation proposes a non-dimensional parameter (Γ) to measure efficiency of piezoelectric sensors mounted on plane surfaces whenever the requirement of thin bonding and sensor layers is satisfied and the condition of perfect parallelism between external surface and sensor is met. Even for reasonable quality bonding the output voltage can present discrepancies of about 10% in comparison to the theoretical voltage assuming perfect bonding (V_∞).

It was shown that the mechanism behind loss of efficiency is due to edge effects on the strain distributions. These may be minimized if tapered bonding layer constructions are allowed. In this way the sharp surfaces illustrated in Figs. 7a-c would display smoother gradient variations, bringing the real output voltage closer to the theoretical one.

A basic discussion on shape effects of the piezoelectric sensors has been given suggesting that some kind optimal criterion may be adopted. The proposed criterion is maximization of the efficiency V/V_∞ considering constant mass. A possible undesirable side effect of working with arbitrarily shaped piezoelectric sensors is that non-idealities in terms of electric field distribution (leakage for example) may become relevant if the optimal design obtained has a highly non-convex shape.

7. References

- Allik, H. and Hughes, T. J. R., 1970, "Finite Element Method for Piezoelectric Vibration", *Int. Journal for Numerical Methods in Engineering*, Vol. 2, pp. 151-157.
- Barrett, R., 1994, "Active Plate and Missile Wing Development Using Directionally Attached Piezoelectric Elements", *AIAA Journal*, Vol. 33, No. 2, pp. 601-609.
- Batra, R. C. and Liang, X. Q., 1996, "Shape Control of Vibrating Simply Supported Rectangular Plates", *AIAA Journal*, Vol. 34, No. 1, pp. 116-132.
- Crawley, E. F. and Anderson, E. H., 1990, "Detailed Models for Piezoelectric Actuation of Beams", *Journal of Intelligent Material Systems and Structures*, Vol. 1, pp. 4-25.
- Crawley, E. F. and de Luis, J., 1987, "Use of the Piezoelectric Actuators as Elements of Intelligent Structures", *AIAA Journal*, Vol. 25, No. 10, pp. 1373-1385.
- de Faria, A. R. and de Almeida, S. F. M., 1996, "Modeling of Actively Damped Beams with Piezoelectric Actuators with Finite Stiffness Bond", *Journal of Intelligent Material Systems and Structures*, Vol. 7, No. 6, pp. 677-688.

- Ha, S. K., Keilers, C. and Chang, F. K., 1992, "Finite Element Analysis of Composite Structures Containing Distributed Piezoelectric Sensors and Actuators", *AIAA Journal*, Vol. 30, No. 3, pp. 772-780.
- Liao, C. Y. and Sung, C. K., 1991, "Vibration Suppression of Flexible Linkage Mechanisms Using Piezoelectric Sensors and Actuators", *Journal of Intelligent Material Systems and Structures*, Vol. 2, pp. 177-197.
- Meressi, T. and Padent, B., 1993, "Buckling Control of a Flexible Beam Using Piezoelectric Actuator", *Journal of Guidance, Control and Dynamics*, Vol. 16, No. 5, pp. 977-980.
- Nabarrete, A., 2002, "A Three Layer Quasi 3D Finite Element Model for Structural Analysis of Sandwich Plates", Doctoral thesis, Instituto Tecnológico de Aeronáutica (ITA).
- Trindade, M. A., Benjeddou, A. and Ohayou, R., 2000, "Modeling of Frequency Dependent Viscoelastic Materials for Active-Passive Vibration Damping", *Transactions of ASME, Journal of Vibration and Acoustics*, Vol. 122, No. 2, pp. 169-174.
- Trindade, M. A., Benjeddou, A. and Ohayou, R., 2001, "Finite Element Modeling of Hybrid Active-Passive Vibration Damping of Multilayer Piezoelectric Sandwich Beams Part 1: Formulation", *International Journal for Numerical Methods in Engineering*, Vol. 51, No. 7, pp. 835-854.
- Tzou, H. S., 1991, "Distributed Model Identification and Vibration Control of Continua: Theory and Applications" *Applied Mechanics Review*, Vol. 118, No. 3, pp. 494-499.

8. Copyright Notice

The author is the only responsible for the printed material included in his paper.